ChemCatChem

Research Article
doi.org/10.1002/cctc.202301174

Chemistry Europe
European Chemical Societies Publishing

www.chemcatchem.org

MnFeNi-Based Composite as a Case Study of a Bifunctional Oxygen Electrocatalyst under Dynamically Changing Electrode Potentials

Dulce M. Morales,*[a, b] Mariya A. Kazakova,[c] Danea Medina,[c] Javier Villalobos,[b] Götz Schuck,[d] Marcel Risch,[b] and Wolfgang Schuhmann[c]

High-performance bifunctional electrocatalysts for the oxygen reduction (ORR) and oxygen evolution reaction (OER) are essential components in energy conversion and storage technologies. Yet, their poor reversibility hinders their applicability. A highly active ORR/OER catalyst, consisting of multiwalled carbon nanotubes-supported MnFeNiOx nanoparticles, was subjected to sequences of chronoamperometric steps alternating between the ORR, the OER and highly cathodic potentials (E_c). Rotating ring disk electrode methods revealed that applying E_c leads to a small increase in the current and peroxide species yield during the ORR while enhancing substantially the OER. X-ray absorption spectroscopy showed irreversible changes in the chemical state of MnFeNiOx correlating with its catalytic properties. The complexity of changes that a composite catalyst may undergo under varying potentials, the importance of monitoring product formation, and the convenience of using dynamic electrochemical sequences for the assessment of catalyst reversibility, as well as for the activation and/or restoration of their catalytic properties, are highlighted.

Introduction

Bifunctional oxygen electrodes (BOEs) are electrocatalytic materials that reversibly exhibit high performance towards the oxygen evolution reaction (OER) and the oxygen reduction reaction (ORR), and are essential components of energy conversion and storage devices such as unitized fuel cell/electrolyzers and rechargeable metal-air batteries.[1] Finding suitable, low-cost electrocatalysts for reversible oxygen conversion is crucial for the development and widespread application of these environmentally friendly technologies. BOEs typically comprise a combination of ORR and OER active sites brought together into a composite material.[2] A wide variety of highly active ORR/OER catalysts has been reported,[3] including both precious metal-containing[4] and precious metal-free materials,[5] very often comprising more than one metal component as well as a conductive support, typically carbon-based materials,[6] metal foams[7] or metal nanowires.[8] Hence, high-performance ORR/OER catalysts reported to date consist of complex composite materials[1] such as metal organic frameworks and metal organic polymers,[9] metal oxide nanoparticles supported onto or embedded within heteroatom-doped nanostructured carbons,[10, 11] carbon-encapsulated metal alloys,[12] aerogel-based hybrids,[13] among others, with their different components contributing synergistically to their catalytic properties. However, it is frequently observed that highly active BOEs exhibit poor stability at alternating ORR/OER conditions, even if these catalysts are stable when the OER and the ORR are conducted separately.[14,15] Such materials are unsuitable for applications that require operation under dynamic ORR/OER conditions as it is for reversible energy conversion and storage devices.[16] Different strategies have been proposed with the aim of preventing activity loss of BOEs at alternating ORR/OER conditions, including the use of decoupled electrochemical cell configurations where the ORR and OER electrode films are used independently from each other,[10,17] the exploitation of synergistic effects between metal components in the ORR and OER active sites,[11,14,18] the fine control of size and distribution of catalyst particles embedded within the catalyst support,[19,20] and the incorporation of stability promoters into catalyst composites.[21] Corrective strategies have also been explored with the aim of restoring, at least partially, the catalytic properties of oxygen electrocatalysts after operation. Examples include the exploitation of self-repair mechanisms,[22] and the deliberate variation of applied electrode potentials to allow for

[a] Dr. D. M. Morales
Engineering and Technology Institute Groningen (ENTEG), University of Groningen
Nijenborgh 4, Groningen 9747AG, The Netherlands
E-mail: d.m.morales.hernandez@rug.nl

[b] Dr. D. M. Morales, Dr. J. Villalobos, Dr. M. Risch
Nachwuchsgruppe Gestaltung des Sauerstoffentwicklungsmechanismus, Helmholtz-Zentrum Berlin für Materialien und Energie GmbH
Hahn-Meitner-Platz 1, 14109 Berlin, Germany

[c] Dr. M. A. Kazakova, Dr. D. Medina, Prof. Dr. W. Schuhmann
Analytical Chemistry – Center for Electrochemical Sciences (CES), Faculty of Chemistry and Biochemistry, Ruhr University Bochum
Universitätsstr. 150, 44780 Bochum, Germany

[d] Dr. G. Schuck
Abteilung Struktur und Dynamik von Energiematerialien, Helmholtz-Zentrum Berlin für Materialien und Energie GmbH
Hahn-Meitner-Platz 1, 14109 Berlin, Germany

Supporting information for this article is available on the WWW under https://doi.org/10.1002/cctc.202301174

the diffusion of gas bubbles[23,24] and/or the regeneration of active sites.[25, 26] The success of any of these different strategies, however, depends largely on the nature of the catalyst and on the specific cause of activity loss. Yet, identifying the deactivation mechanisms of multicomponent materials, such as carbon-supported multi-metallic composites, remains a major challenge in their investigation and further development due to their complex nature.

In a previous work,[26] a corrective approach to recover the catalytic capabilities of an Fe/NC-based ORR catalyst after exposure to anodic potentials was presented. The approach consisted of applying short highly-reductive potential pulses with the aim of reverting the oxidation of the active sites that may occur during the OER. We hypothesize that a similar approach can be applied to revert the oxidative damage that the BOE's active sites undergo during OER operation. Furthermore, it has been shown that variation of the electrode potential may also lead to changes in the structure and/or surface state of OER catalysts that can be exploited as electrochemical activation procedures.[27–29] Thus, the study of BOEs under conditions with dynamically changing electrode potentials has an enormous potential of revealing ways to enhance, *in situ*, the activity and also the much-needed bifunctional stability of this type of catalytic materials.

Herein, we investigate a previously reported BOE,[10] hereafter denoted MnFeNiOx, which consists of metal oxide nanoparticles embedded in oxygen-functionalized multiwalled carbon nanotubes (MWCNTs). A thorough structural characterization of this catalyst has been reported earlier[10] and is summarized in Table S1. In brief, the total metal loading in MnFeNiOx is 14.4 wt% (Mn = 7.3 wt%, Fe = 2.1 wt%, and Ni = 5.0 wt%) according to X-ray fluorescence (XRF). High resolution transmission electron microscopy (HR-TEM) revealed that the metal oxide nanoparticles distributed inside (56%) and outside (44%) the MWCNTs have average particle sizes of 3.6 ± 1.2 nm and 10.5 ± 5.9 nm, respectively. The crystal structure of the metal oxide nanoparticles was investigated by X-ray diffraction (XRD), revealing a highly defective, multiphasic structure. The main phases identified included NaCl-type NiO, and spinel-type Fe_3O_4, Mn_3O_4, $MnFe_2O_4$, $NiFe_2O_4$ and $NiMn_2O_4$. The main surface species in the as-prepared MnFeNiOx material were identified by X-ray photoelectron spectroscopy (XPS) and included Mn^{2+}, Mn^{3+}, Ni^{2+} and Fe^{3+}, in agreement with XRD results. Moreover, the composite exhibited a specific surface area of 263 $m^2 g^{-1}$ and an average double layer capacitance of 7.6 mF cm^{-2} determined by scan rate-dependent cyclic voltammetry. Evaluation of the bifunctional ORR/OER activity of MnFeNiOx by rotating disk electrode (RDE) voltammetry revealed that the catalyst exhibited a ΔE value of 0.73 V, determined as the difference between the potentials recorded at $+10$ mA cm^{-2} and at -1 mA cm^{-2} for the OER and for the ORR, respectively, which was comparable to the ΔE value calculated with RuOx for OER (at $+10$ mA cm^{-2}) and Pt/C for ORR (at -1 mA cm^{-2}) measured under the same conditions.[10] Additionally, MnFeNiOx displayed a stable OER performance during electrolysis conducted alternatingly at $+10$ mA cm^{-2} and a -1 mA cm^{-2} for a total of 10 h,[10] as well as a favorable selectivity towards the direct reduction from O_2 to OH^- via the 4-electron transfer pathway in the presence of ~0.1 wt% Nafion as a binder.[30] Nevertheless, a major obstacle to the applicability of this catalyst is related to its stability, as it exhibited severe loss of ORR activity under alternating ORR/OER operating conditions.[10] Here, we propose that the observed decline in activity of MnFeNiOx is due to oxidation of ORR active sites upon exposure to the anodic potentials of the OER, in which case applying short, highly cathodic potential pulses could potentially lead to a recovery of its ORR catalytic capabilities. MnFeNiOx is a particularly interesting material to conduct this investigation since the deactivation of the ORR sites occurs fast under alternating ORR/OER potentials, while the OER performance remains unchanged during stability tests, indicating also a sufficient resistance of the MWCNTs to carbon corrosion under the employed conditions.[10] Here, we use three different electrochemical challenges during which the potentials are dynamically changed with the purpose of exposing the catalyst either to (i) ORR conditions, (ii) alternatingly to ORR and OER conditions, and (iii) the latter including short highly cathodic potential pulses before applying again the ORR potential within the sequence. We investigate the changes in the bifunctional ORR/OER activity and selectivity that the catalyst undergoes upon its exposure to these sequences by means of electrochemical methods using a rotating ring disk electrode (RRDE) setup to detect ORR and OER products. Furthermore, we correlate these results to changes in the average chemical state of Mn, Fe and Ni in the catalyst determined by X-ray absorption spectroscopy. This work illustrates the complexity of changes that a catalyst may undergo under dynamically changing electrode potentials, and the wide ground for opportunity to exploit these changes for enhancing the performance of BOEs *in situ*.

Results and Discussion

Variation of the ORR/OER activity of MnFeNiOx in terms of current density over time was observed using three different electrochemical sequences, namely (i) E_n/E_{ORR}, (ii) $E_n/E_{ORR}/E_{OER}$ and (iii) $E_n/E_{ORR}/E_{OER}/E_c$, each of them involving a different sequence of chronoamperometric potential steps as depicted in Scheme 1. The applied potentials were dynamically varied to alternate between conditions at which neither the ORR nor the OER takes place (E_n), and at which either the ORR (E_{ORR}) or the OER (E_{OER}) take place. In the case of the sequence (iii) $E_n/E_{ORR}/E_{OER}/E_c$, a step of short highly cathodic potential pulses (E_c) was also applied alternatingly with E_n.

The potentials (vs RHE) selected for MnFeNiOx were $E_n = 1.21$ V (near open circuit potential, where neither the ORR, nor the OER take place), $E_{ORR} = 0.84$ V (corresponding to a current density of about -1 mA cm^{-2}), and $E_{OER} = 1.53$ V (corresponding to a current density of about $+1$ mA cm^{-2}), determined from previously reported ORR and OER polarization curves[10] (also shown in Figure S1). With these relatively low current densities, on the one hand, mainly kinetically-limited ORR currents are observed,[31] and on the other hand, severe blocking of the

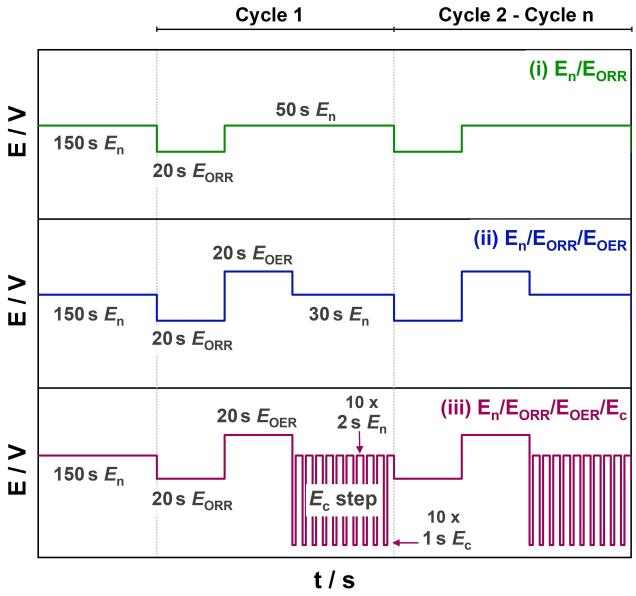

Scheme 1. Representation of three chronoamperometric sequences showing the variation of applied potentials as a function of time. The sequences involve a potential where no oxygen conversion (ORR or OER) takes place (E_n), a potential at which selected current density values are achieved for the ORR (E_{ORR}) and for the OER (E_{OER}), and a highly cathodic potential (E_c).

surface due to O_2 bubbles formed during the OER is avoided. Additionally, stability issues due to vigorous bubble formation (i.e., catalyst detachment) and carbon corrosion are also avoided, facilitating thus the observation of effects related to metal oxidation/reduction during the electrochemical tests.

In a previous work, an approach to mitigate the damage of the catalytic sites in an Fe/NC-based ORR catalyst caused by exposure to relatively high anodic potentials (1.8 V vs RHE) was presented. The approach consisted of repeatedly applying short cathodic pulses (2.3 s) between 0.50 and −0.88 V vs RHE. It was shown that the activity of this catalyst could be partially restored upon optimization of these pulses (optimal value was −0.13 V vs RHE), thus prolonging its lifetime as an ORR electrocatalyst.[26] Additionally, it was found that in most cases the effect of applying the cathodic pulse could only be observed after a few repetitions. Taking these findings as our starting point, we fixed the duration of the E_c pulses to 1 s and the number of repetitions to 10 for the E_c step for all experiments performed here. Between each E_c pulse, E_n was applied for 2 s to allow the species formed upon applying E_c to be forcedly convected from the surface of the electrode upon rotation at 1600 rpm. Only the last point measured during the E_{ORR} and E_{OER} potential steps was considered for the analysis to minimize capacitive contributions.

A preliminary estimation of the optimal E_c value for MnFeNiOx consisted in screening a wide range of E_c values in a single experiment by using the sequence (iii) $E_n/E_{ORR}/E_{OER}/E_c$ and varying the E_c values between 0.37 and −0.53 V vs RHE. Each E_c step was applied for a total of 5 cycles before increasing the potential to the next (more cathodic) value in 100 mV steps. To observe the effect of the E_c step, the sequences (i) E_n/E_{ORR} and (ii) $E_n/E_{ORR}/E_{OER}$ were conducted repeatedly for a total number of cycles that matched that of (iii) $E_n/E_{ORR}/E_{OER}/E_c$ to ensure that the measurements have the same total duration, and thus, the same exposure time to the ORR and OER conditions. As shown in Figure 1a, most of the screened E_c values (indicated with color bars in the figure) are more positive than the overpotential region of the hydrogen evolution reaction (HER). Namely, HER currents were only clearly distinguished from the baseline at potentials more negative than −0.3 V vs RHE. All measurements were conducted at least three times using freshly prepared electrodes to observe their reproducibility. The net currents measured during each of the repetitions were slightly different to each other, which can be attributed to differences in the electrode films due to drop-casting, as well as to variations in the uncompensated resistance (R_u = 49–58 Ω).

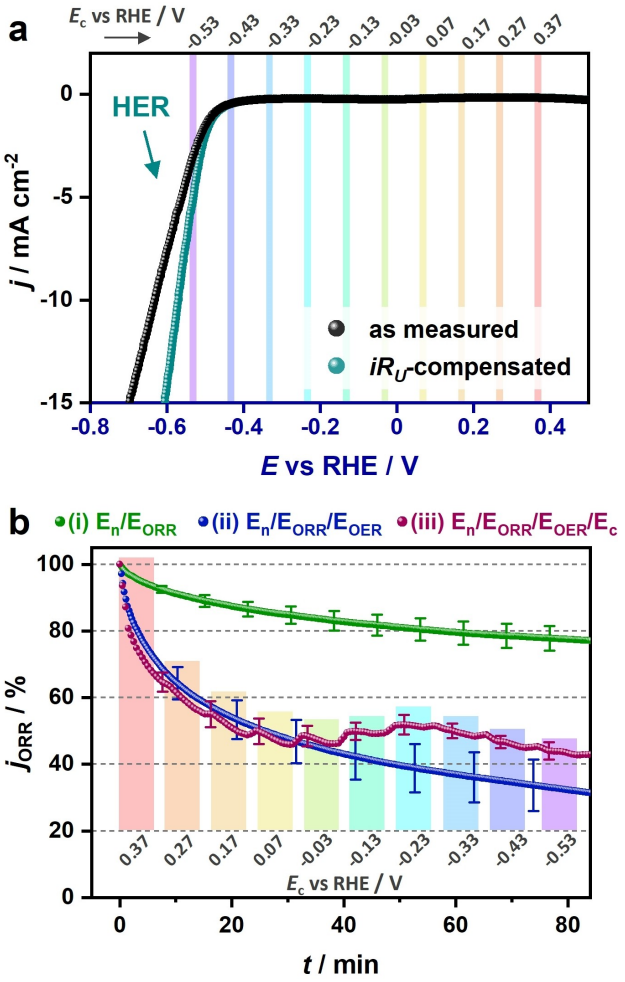

Figure 1. (a) Linear sweep voltammetry of MnFeNiOx recorded in Ar-saturated 0.1 M KOH at 5 mV s^{-1} scan rate and 1600 rpm electrode rotation. Potentials are shown as measured (black) and after iR_U-drop compensation (teal, R_U = 54 Ω). (b) Percentage of current density measured at the end of every E_{ORR} step with respect to the current density measured at the end of the first E_{ORR} step (j_{ORR}) recorded during the three chronoamperometric sequences indicated in Scheme 1. Error bars represent the standard deviation of 3 independent measurements. Tests were conducted in O_2-saturated 0.1 M KOH at 5 mV s^{-1} scan rate and 1600 rpm electrode rotation. Potentials (vs RHE) applied were E_n = 1.20 V, E_{ORR} = 0.83 V and E_{OER} = 1.52 V. E_c was varied from 0.37 to −0.53 V in 100 mV steps every 5 cycles, and its values are indicated with bars of the same color in the two figures to facilitate their visualization.

The currents also differed from the target $+1\ mA\,cm^{-2}$ (OER) and $-1\ mA\,cm^{-2}$ (ORR), due to the aforementioned factors in addition to small differences in the applied potentials with respect to the reference voltammograms reported in our previous work[10] when converting the selected E vs RHE values to the reference electrode scale (the potentials applied with respect to the reference electrode are summarized in Table S2). Despite the differences in the applied electrode potentials and the net currents measured, the trends observed were reproducible for all repeated experiments. To facilitate the comparison between the different measurements, the current densities (j) measured at the E_{ORR} and E_{OER} steps during each of the sequences were normalized with respect to their corresponding current density values measured at the first cycle (j_i), and were expressed in terms of percentage (here denoted j_{ORR} and j_{OER}, respectively). A representative example is presented in Figure S2 showing j values recorded at the E_{ORR} step for a set of four measurements (Figure S2a) and the corresponding j_{ORR} values obtained after normalization (Figure S2b).

Figure 1b shows the average j_{ORR} values (the average of the different repetitions) as a function of time corresponding to each of the chronoamperometric sequences indicated in Scheme 1 to highlight the stability trends.[32] Note that the color bars indicated in Figure 1b correspond to those in Figure 1a and represent the screened E_c values. Comparison between the j_{ORR} values observed during (i) E_n/E_{ORR} (green) and (ii) $E_n/E_{ORR}/E_{OER}$ (dark blue) clearly shows that the decline of activity was substantially more severe in the case of the latter, displaying a j_{ORR} of 50% after about 25 min, and retaining only about one third of the initial current density after 80 min, whereas the electrode exposed to the sequence (i) E_n/E_{ORR} (in which case the catalyst was not exposed to the OER potential) exhibited a j_{ORR} of ~78% after 80 min. In the case of the sequence (iii) $E_n/E_{ORR}/E_{OER}/E_c$, j_{ORR} values coincided within experimental error with those observed with (ii) $E_n/E_{ORR}/E_{OER}$ during the first ~35 min, which corresponds to scanned E_c values in the range between 0.37 and −0.03 V vs RHE. These results suggest that, within this potential range, the E_c step —using 10 repetitions and 1-second-long cathodic pulses— does not have a substantial effect on the ORR stability of MnFeNiOx at alternating ORR/OER conditions. Meanwhile, using E_c values equal or more cathodic than −0.13 V vs RHE led to a clear increase in j_{ORR}. While this could indicate that a partial recovery of the ORR activity is taking place (according to our hypothesis), it is also possible that the increase in current is due to an oxidation process taking place during the E_{ORR} step after having applied the more cathodic E_c potential pulse. In other words, it could be the case that one or more of the metals in MnFeNiOx could have undergone reduction due to E_c which was then reverted during the E_{ORR} step, thus leading to an increase in current. Maximum increase in j_{ORR} was achieved with $E_c = -0.23$ V vs RHE, observing a j_{ORR} of about 52% at t = 50 min, whereas j_{ORR} was ~39% for the sequence (ii) $E_n/E_{ORR}/E_{OER}$ (with no E_c step) at the same measuring time. Apparently, applying more cathodic E_c values did not lead to further recovery of the measured current density.

This first E_c-scanning approach offers a fast estimation of the potential range at which E_c could be effective in restoring, at least partially, the currents measured during the E_{ORR} step. This method is highly convenient compared to the time-consuming approach of conducting multiple measurements at a single E_c value (particularly if a wide range of E_c values needs to be evaluated), and can be easily applied to other ORR/OER materials to reveal, with a single experiment, whether applying cathodic pulses could lead to an activity enhancement. However, it is important to note that the most cathodic E_c pulses were only applied at longer measuring times, and it is likely that a higher recovery of j_{ORR} could be achieved with E_c values different to the apparent optimal ($E_c = -0.23$ V vs RHE) if they had been applied from the beginning of the test. Thus, MnFeNiOx was subjected to the chronoamperometric sequence (iii) $E_n/E_{ORR}/E_{OER}/E_c$ using fixed E_c values (vs RHE) of 0.07 V (300 mV less negative than the apparent optimal E_c value), −0.23 V (the apparent optimal E_c value), and −0.53 V (300 mV more negative than the apparent optimal E_c value). The sequences were conducted continuously for a total duration of 100 min. The average j_{ORR} profiles obtained from at least two measurements are shown in Figure 2, and are also compared to those obtained during the sequences (i) E_n/E_{ORR} (green) and (ii) $E_n/E_{ORR}/E_{OER}$ (dark blue). The average of the j_{ORR} values obtained by the end of the experiments (at t = 100 min) for each of the sequences are summarized in Table S3.

As shown in Figure 2, using the least cathodic E_c value of 0.07 V vs RHE did not lead to a substantial difference in the j_{ORR} profile with respect to that of the sequence (ii) $E_n/E_{ORR}/E_{OER}$ where no E_c pulse was applied. Yet, mitigation of the current loss was indeed observed with more negative E_c values. Additionally, the retained relative current was slightly but insignificantly higher using $E_c = -0.53$ V vs RHE than it was with $E_c = -0.23$ V vs RHE, achieving average j_{ORR} values of 42% and

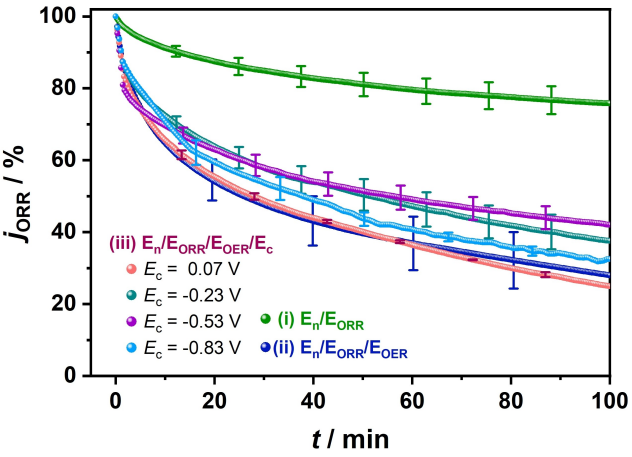

Figure 2. Current density measured at the end of the E_{ORR} step in each cycle with respect to the current density measured at the end of the E_{ORR} step of the first cycle (j_{ORR}) recorded during the two chronoamperometric sequences indicated in Scheme 1. Error bars represent the standard error of at least three independent measurements. Tests were conducted in O_2-saturated 0.1 M KOH at 5 $mV\,s^{-1}$ scan rate and 1600 rpm electrode rotation. Potentials (vs RHE) applied were $E_n = 1.20$ V, $E_{ORR} = 0.83$ V and $E_{OER} = 1.52$ V. E_c values used for the sequence (iii) $E_n/E_{ORR}/E_{OER}/E_c$ are indicated in the figure.

38%, respectively, by the end of the test (t = 100 min). This suggests that the optimal E_c value identified from our initial E_c-scanning approach (−0.23 V vs RHE, Figure 1b) is different to the optimal value identified when using an unchanging E_c value throughout the experiment (−0.53 V vs RHE, Figure 2). Likely, by the time E_c = −0.53 V vs RHE was applied in the experiment shown in Figure 1b, a high degree of oxidative damage was already done to MnFeNiOx compared to E_c = −0.23 V vs RHE, which was applied at an earlier time during the measurement. This observation further suggests that the restoring effect of E_c does not only depend on its value (and its duration[33]), but it is also hysteretic, namely, its effectiveness depends on the history of the electrode film. From the previous observation, it can be assumed that an even more negative E_c pulse may lead to a more substantial increase in j_{ORR}. To confirm if this is the case, an additional set of measurements was conducted using an E_c pulse of −0.83 vs RHE (300 mV more negative than the most cathodic E_c screened in Figure 1b). Interestingly, as observed in the corresponding j_{ORR} profile in Figure 2, applying this more negative E_c resulted in lower j_{ORR} values compared to both E_c values −0.23 and −0.53 V vs RHE. Yet, it is important to consider that hydrogen bubbles are formed vigorously at −0.83 vs RHE (Figure 1a), which may lead to an apparently decreased current due to substantial blocking of the electrode surface.[26] From the set of experiments shown in Figure 2, −0.53 V vs RHE was identified as the optimal E_c value in terms of its effectiveness to mitigate the current density loss after 100 min measurement. Thus, E_c was fixed to this value for the subsequent investigations. It is important to mention that further optimization is still possible not only in terms of the value of E_c but also in terms of its duration and the number of repetitions of E_c within the sequence (iii) $E_n/E_{ORR}/E_{OER}/E_c$.

To further investigate the impact that the different dynamic potential sequences have on the ORR activity and selectivity of MnFeNiOx, linear sweep voltammograms were collected before and after subjecting the catalyst to each sequence for a total of 20 cycles (~30 min) using a rotating ring disk electrode (RRDE) setup, which allows to monitor the formation of peroxide species during the ORR. It is noteworthy that the chronoamperometric experiments shown earlier in Figure 2 and the voltammetric experiments that are discussed in the following are not directly comparable due to the large differences in both their timescales and potential ranges. Linear sweep voltammetry is used here for observing the irreversible impact of the three different chronoamperometric sequences on the catalytic properties of MnFeNiOx towards the ORR. Figure 3a shows overlapping polarization curves obtained with three MnFeNiOx electrode films before subjecting them to either of the three sequences, indicating a high reproducibility of the experiments (including the electrode preparation method). Conversely, the voltammograms recorded after the chronoamperometric tests displayed major differences (Figure 3b). It is important to note, however, that differences observed in the diffusion-control and kinetic-control voltammetric regions may be different in nature. For a clear visualization, Figure S3 shows a zoomed-in version of Figure 3b that facilitates the comparison of the voltammograms in the kinetic-control region. In agreement with the

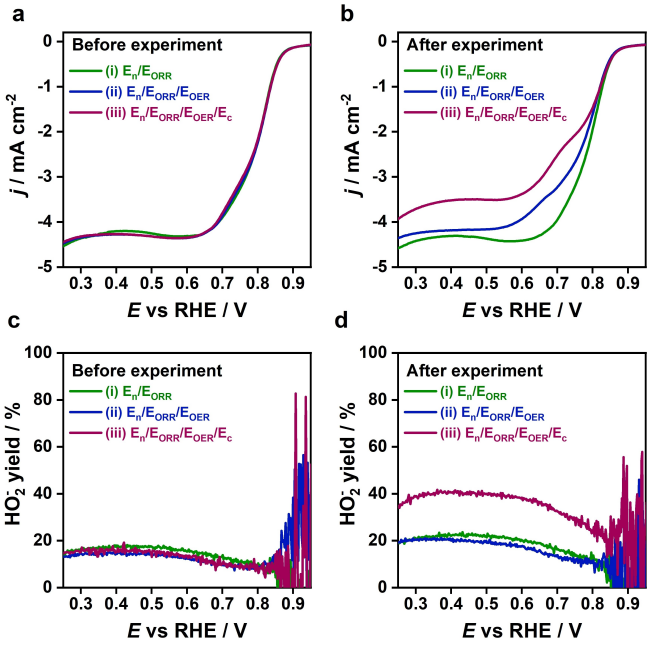

Figure 3. Linear sweep voltammograms of MnFeNiOx recorded in the ORR potential region (a) before and (b) after the three chronoamperometric sequences indicated in Scheme 1, and their (c,d) corresponding yields of peroxide species (HO_2^-) as a function of the electrode potential. Measurements were conducted in O_2-saturated 0.1 M KOH and 1600 rpm electrode rotation. Voltammograms were recorded with 5 mV s^{-1} scan rate, maintaining a ring electrode potential of 1.37 V vs RHE for the detection of peroxide species. Potentials (vs RHE) applied during the chronometric sequences were E_n = 1.20 V, E_{ORR} = 0.83 V, E_{OER} = 1.52 V, and E_c = −0.53 V.

observations made in relation to Figure 1 and 2, the catalytic properties of MnFeNiOx were preserved the most when the catalyst was not exposed to the anodic conditions of the OER, that is, with the sequence (i) E_n/E_{ORR}. Meanwhile, in the case of (ii) $E_n/E_{ORR}/E_{OER}$, an increase in the overpotential (Figure S3) and a decrease in the diffusion-limited current density towards more positive values (Figure 3b) were observed. Interestingly, at current densities up to about −0.5 mA cm^{-2}, the ORR overpotentials recorded after the sequence (iii) $E_n/E_{ORR}/E_{OER}/E_c$ resembled those obtained after (i) E_n/E_{ORR}, while at higher (more negative) current densities the overpotentials increased (Figure S3b). Furthermore, the change in the diffusion-limited current was more substantial in the case of the sequence involving E_c.

Changes in the shapes of the voltammograms after the sequences (ii) $E_n/E_{ORR}/E_{OER}$ and (iii) $E_n/E_{ORR}/E_{OER}/E_c$, particularly in the potential range between 0.6 and 0.8 V vs RHE, were also observed. The differences in the features of the ORR curves are explained by the multi-site nature of MnFeNiOx, comprising not only a variety of multiphase mono- and bimetallic highly defective oxides according to XRD[10] but also the surface of the mildly oxidized carbon nanotubes, which altogether contribute to the ORR activity.[20] Thus, the differences in the voltammetric responses after the three sequences are a result of a distribution of different types of active sites, each with a different maximum turnover,[34] which in addition are likely to be affected differently by either or both the E_c and the E_{OER} steps.

Changes in the diffusion-limited current suggest that the different chronoamperometric sequences may have an impact on the ORR selectivity of MnFeNiOx. To ascertain if this is the case, and whether this is caused by E_{OER}, by E_c or by both, the yields of peroxide species (HO_2^-) produced during the ORR scans were determined. As shown in Figure 3c, before conducting any of the three sequences, the three MnFeNiOx films displayed reproducible profiles for HO_2^- yield as function of the applied potential, with a maximum yield of ~15%, indicating a preferred 4-electron transfer pathway in agreement with our previous report.[30] Interestingly, the HO_2^- yield vs potential profiles obtained after the sequences (i) E_n/E_{ORR} and (ii) $E_n/E_{ORR}/E_{OER}$ displayed similar changes (Figure 3d), with an increase in the maximum peroxide yield to ~20%. These results suggest that, regardless of the observed differences in overpotentials and diffusion-limited currents, MnFeNiOx retains its selectivity towards the direct reduction of O_2 to OH^- after each of these two sequences. It can be reasoned that applying the anodic potentials of the OER (during the E_{OER} step) results in more sluggish kinetics and/or lower availability of the active sites in MnFeNiOx, without a strong impact in their selectivity. Contrastingly, substantially larger peroxide yields were observed after the chronoamperometric sequence (iii) $E_n/E_{ORR}/E_{OER}/E_c$, with a maximum HO_2^- yield of ~40% after the test, suggesting that E_c induces a change in the ORR-active species that dominate the ORR selectivity in MnFeNiOx.

At this point, it is also important to assess the impact that the sequences (ii) $E_n/E_{ORR}/E_{OER}$ and (iii) $E_n/E_{ORR}/E_{OER}/E_c$ have on the activity of MnFeNiOx towards the OER. Therefore, the j_{OER} profiles, corresponding to the relative currents measured at the E_{OER} steps duirng the two sequences are shown in Figure 4. The average j_{OER} values obtained after conducting the measurements for 100 min are summarized in Table S3. Note that the j_{OER} profiles shown in Figure 4 are complementary to the j_{ORR} profiles shown in Figure 2, as the two sets of data (the currents from which the relative current densities j_{ORR} and j_{OER} were determined) were recorded during the same experiments. The error bars shown in Figure 4 are larger than those in Figure 2, which can be attributed to partial blockage of the electrode surface during the OER due to the formation of micro and macro-gas bubbles.[35]

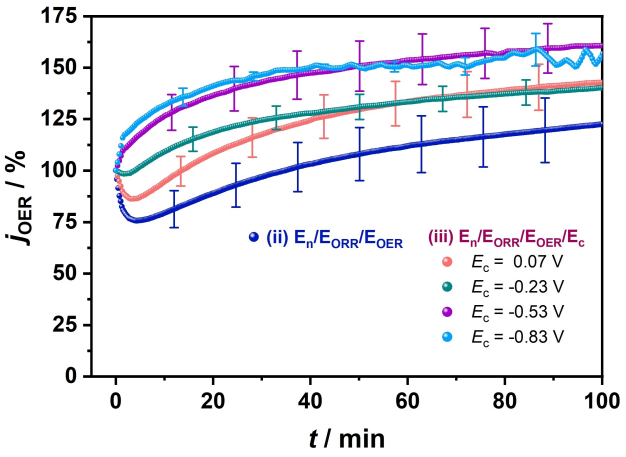

Figure 4. Current density measured at the end of the E_{OER} step in each cycle with respect to the current density measured at the end of the E_{OER} step of the first cycle (j_{OER}) recorded during the sequences (ii) $E_n/E_{ORR}/E_{OER}$ and (iii) $E_n/E_{ORR}/E_{OER}/E_c$ indicated in Scheme 1. Error bars represent the standard error of at least two independent measurements. Tests were conducted in O_2-saturated 0.1 M KOH at 5 mV s^{-1} scan rate and 1600 rpm electrode rotation. Potentials (vs RHE) applied were $E_n = 1.20$ V, $E_{ORR} = 0.83$ V and $E_{OER} = 1.52$ V. E_c values used for sequence (iii) $E_n/E_{ORR}/E_{OER}/E_c$ are indicated in the figure.

In the case of the sequence (ii) $E_n/E_{ORR}/E_{OER}$, the catalyst displayed a decrease in j_{OER} to ~76% during the first minutes, after which it increased, reaching a j_{OER} value of ~122% at t = 100 min. Interestingly, exposing MnFeNiOx to (iii) $E_n/E_{ORR}/E_{OER}/E_c$ with $E_c = 0.07$ or -0.23 V vs RHE led to j_{OER} vs time profiles similar to that of (ii) $E_n/E_{ORR}/E_{OER}$ but with overall higher j_{OER} values. Meanwhile, for the sequences involving more negative E_c values, the catalyst displayed no apparent decrease in j_{OER}, but rather an increase in its value since the first minutes. Furthermore, in these cases, j_{OER} was substantially higher by the end of the measurement than it was during the first cycles. The maximum increase in j_{OER} was observed with $E_c = -0.53$ V vs RHE, reaching a j_{OER} value of about 161% after 100 min. With the most negative E_c (-0.83 V vs RHE), the observed j_{OER} profile was "shakier" compared to less cathodic E_c values, likely due to a considerably higher rate of H_2 formation (HER) taking place at that potential according to Figure 1a, which results in surface blocking and/or catalyst detachment, leading thus to an apparent lower increase in j_{OER} compared to $E_c = -0.53$ V vs RHE.

The observed increases in the relative OER current density (j_{OER}) over time could be explained by an increase in the OER rate, by (re)oxidation of the components in MnFeNiOx, or both. In the first case, higher currents may be due to electrochemically-induced phase transitions of the metal oxide components in MnFeNiOx and/or the formation of more active species.[36, 37] Potential-dependent activation processes have been discussed in detail for hydrous Ni[38] and Fe[39] surfaces in reports by Lyons *et al.*, where it was shown that the potential window during continuous cycling, as well as the scan rate and number of cycles, play an important role in the formation and extent of growth of certain phases. Meanwhile, Radinger *et al.* reported that, by including a chronoamperometric step at 0.8 V vs RHE during the activation procedure of different MnOx films, an enhancement of the OER activity was achieved, which was ascribed to the formation of a highly amorphous mixed-valence oxide.[40] Yet, it is also plausible that the highly reductive E_c pulses lead to the formation of oxygen vacancies, which have been shown to enhance the OER performance of metal oxides via electronic effects that beneficially tune their adsorption properties, electronic conductivity and/or rate limiting step.[41, 42] Therefore, it is likely that alternating between the anodic potentials of the E_{OER} step and the cathodic potentials of the E_{ORR}, and additionally applying E_c, leads to changes in MnFeNiOx that ultimately result in the formation of more active species. For the second case, it is important to consider that the metal components in MnFeNiOx are likely to undergo reduction at the highly cathodic potentials of E_c,[36] in which case a re-oxidization process could take place during the E_{OER} step and contribute (alongside the OER) to the net currents measured.

For that reason, it is necessary to establish whether the increase in j_{OER} (which is determined from the net current measured during the E_{OER} step) is related to an enhancement of the OER rate, to the oxidation of metal species, particularly those formed while applying E_c, or to both. For this purpose, the catalyst was subjected to the sequences (ii) $E_n/E_{ORR}/E_{OER}$ and (iii) $E_n/E_{ORR}/E_{OER}/E_c$ in an Ar-saturated electrolyte using an RRDE setup, which allows monitoring the formation of O_2 during the experiment. Namely, the O_2 produced at the catalyst-modified disk electrode can be reduced (thus detected) at the Pt ring electrode. For a clear visualization of the background currents at both the disk and ring electrodes, E_n was applied for 150 s before and for 150 s after conducting for 20 cycles the corresponding chronoamperometric sequence. The absolute disk ($|j_{disk}|$) and ring ($|j_{ring}|$) current densities recorded during the experiments were plotted as a function of time and are shown in Figure 5a and 5b, respectively. Note that even though the E_{ORR} step is part of the two sequences, oxygen reduction does not actually take place in these experiments since the electrolyte used was oxygen-free.

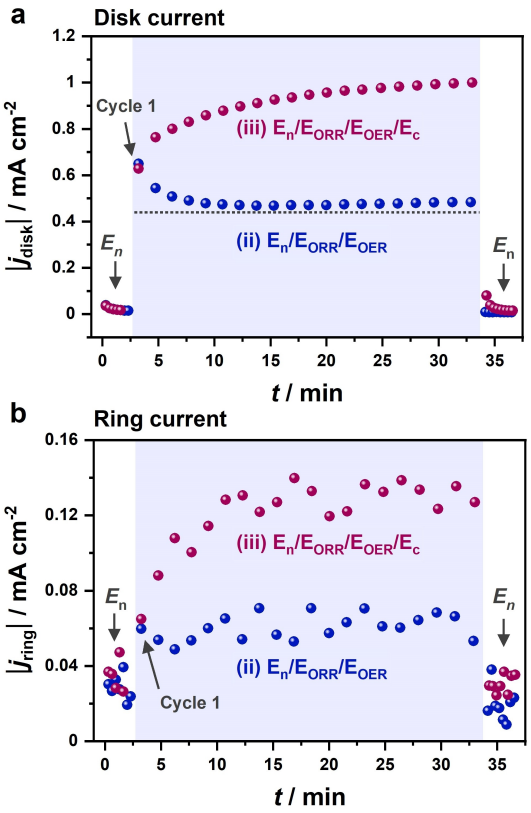

Figure 5. Absolute current densities measured at the (a) disk electrode ($|j_{disk}|$) and (b) ring electrode ($|j_{ring}|$), recorded at the end of each E_{OER} step during sequences (ii) $E_n/E_{ORR}/E_{OER}$ and (iii) $E_n/E_{ORR}/E_{OER}/E_c$. Tests were conducted in Ar-saturated 0.1 M KOH with 1600 rpm electrode rotation. Potentials (vs RHE) applied at the disk were $E_n = 1.20$ V, $E_{ORR} = 0.83$ V, $E_{OER} = 1.52$ V, and $E_c = -0.53$ V. A potential of 0.27 V vs RHE was held at ring electrode throughout the full duration of the experiments to reduce the oxygen produced at the disk electrode. E_n was held for 150 s before and 150 s after completing 20 cycles for a clear visualization of the background currents (shown with a white background). The horizontal dashed line in (a) is included as aid to guide the eye.

In the case of the sequence (ii) $E_n/E_{ORR}/E_{OER}$, the observed $|j_{disk}|$ (Figure 5a, dark blue) decreased during the first minutes and then slightly increased again as the measurement continued, suggesting a similar profile to that of j_{OER} in Figure 4. Meanwhile, the corresponding $|j_{ring}|$ vs time profile (Figure 5b, dark blue), which was clearly distinguishable from the background current, suggested a rather steady current throughout the measurement. The fact that $|j_{disk}|$ exhibits substantial changes while $|j_{ring}|$ does not, indicates that the net currents measured during the E_{OER} step indeed comprises contributions of oxidation processes taking place in addition to the OER, with the former being more substantial during the first minutes of the tests. Interestingly, in the case of the sequence (iii) $E_n/E_{ORR}/E_{OER}/E_c$, the $|j_{disk}|$ and $|j_{ring}|$ profiles follow similar trends, indicating that the increase in the current measured at the disk correlates to an increase in the amount of oxygen produced. While this does not exclude the possibility that additional oxidation processes may be taking place (thus contributing to the net measured currents), it clearly indicates an enhancement of the OER rate during the measurement. Moreover, both $|j_{disk}|$ and $|j_{ring}|$ were considerably larger for the chronoamperometric sequence (iii) $E_n/E_{ORR}/E_{OER}/E_c$ than they were for (ii) $E_n/E_{ORR}/E_{OER}$ for all cycles except the first one (indicated in Figures 5a and 5b with the label "Cycle 1"). According to Scheme 1, the two sequences are identical until the end of the E_{OER} step in Cycle 1, after which either E_n/E_c (10 times) or E_n are applied, respectively. Thus, it can be deduced that the observed increase in the oxygen formation rate during the sequence (iii) $E_n/E_{ORR}/E_{OER}/E_c$ was a consequence of applying E_c.

The conducted RDE and RRDE experiments showed that subjecting MnFeNiOx to the dynamic potential sequence that involves applying highly cathodic potential pulses E_c led, on the one hand, to a partial recovery of the currents measured during the E_{ORR} step alongside a substantial change in the ORR selectivity (Figures 2 and 3), and on the other hand, to a clear enhancement of the OER activity (Figures 4 and 5). Changes in the ORR/OER activity, as well as in the ORR selectivity caused by the deliberate variation of electrode potential have been previously reported for a variety of earth abundant transition metal-based catalysts, and have been ascribed to different effects, including changes in metal valence, phase transitions and/or amorphization, variations in morphology and surface area, formation of oxygen vacancies, as well as blocking of the electrode surface due to gas bubbles.[14, 24, 26, 28, 29, 41, 43] In the case of MnFeNiOx, bubble formation during OER (during the E_{OER} step) and during HER (using the most cathodic E_c values) seems to have an influence in the observed currents as well as in the reproducibility of the measurements, as discussed earlier. However, the differences observed between the three sequences cannot be fully explained by this. Meanwhile, due to the hybrid nature of the catalyst, surface area effects are difficult to discern. Namely, the catalyst consists of small metal oxide nanoparticles with a distribution of particle sizes that depends on their location (3.6 ± 1.2 nm and 10.5 ± 5.9 nm, inside and outside the MWCNTs, respectively[10]), and that are supported on a high-surface area carbon support, altogether limiting the possibility of observing changes in surface area or morphology

of the individual components. Yet, we established in an earlier study[30] that the Mn valence plays a major role in the ORR selectivity of MnFeNiOx, while we hypothesized that the Fe–Ni couple was mainly responsible for oxygen evolving properties of the catalyst. We thus speculate that, from the different possible effects that E_c has on MnFeNiOx, those leading to the changes observed in the ORR and the OER properties are more substantially related to changes in metal valence, likely accompanied by phase transitions. Therefore, in the following, we focused our study on the investigation of irreversible changes in the chemical state of the metal components of MnFeNiOx after having been exposed to the three chronoamperometric sequences. To achieve this, we resorted to X-ray absorption spectroscopy (XAS) since it is a highly sensitive technique and, in contrast to diffraction-based techniques, XAS offers the possibility of observing the average metal valence(s) in a catalyst regardless of the presence and/or formation of amorphous phases.[44]

XAS spectra were recorded for the as-prepared MnFeNiOx powder and for the catalyst after having been exposed to each of the sequences shown in Scheme 1 for a total of 20 cycles, subsequently applying E_n for 150 s. It is important to consider that our electrode preparation sequence involves dispersing the catalyst in the presence of Nafion followed by ink-deposition, drying, and a conditioning step. The latter consists of recording cyclic voltammograms until an unchanged response is observed (see details in the Experimental section). An example of typical voltammetric responses of MnFeNiOx recorded during this step is shown in Figure S4. Since both the presence of Nafion[30] and the electrochemical conditioning step may have an impact on the chemical state of the metal components in MnFeNiOx, we also recorded XAS spectra of MnFeNiOx after completing the full electrode preparation sequence (denoted here as "after conditioning") without conducting any other electrochemical treatment.

The spectra of the X-ray absorption near edge structure (XANES) collected in the Mn, Ni and Fe K-edges are shown in Figure 6a, 6b and 6c, respectively, and were used to estimate the chemical state of the metal components of the different MnFeNiOx samples (Table 1). For this purpose, XAS spectra of commercial metal oxides (MnO, Mn_2O_3, MnO_2, FeO, Fe_3O_4, Fe_2O_3, NiO and $LiNiO_2$) were collected and the linear regressions of their nominal valences with respect to their corresponding edge energies were obtained as shown in Figure S5. The latter were determined by the step integral method proposed by Dau *et al.*[45] With the resulting linear equations, the metal valences of the reference powders were estimated and are summarized in Table S4 alongside their corresponding nominal valences. Considering that the difference between the nominal and the estimated valences of the reference samples is consistently +/−0.1, we used this approach to qualitatively identify notable differences between the various MnFeNiOx samples, rather than to accurately determine their chemical states. As shown in Table 1, the average metal valences in the as-prepared MnFeNiOx sample are 3.0, 3.0 and 2.8 for Mn, Fe and Ni, respectively. Interestingly, as shown in Figures 6a, 6b and 6c, all three metals in MnFeNiOx underwent irreversible oxidation after conditioning, highlighting the importance of the careful selection of sample preparation protocols including conditioning and/or activation sequences.

To facilitate the comparison between the as-prepared catalyst and the different electrochemically treated samples, the

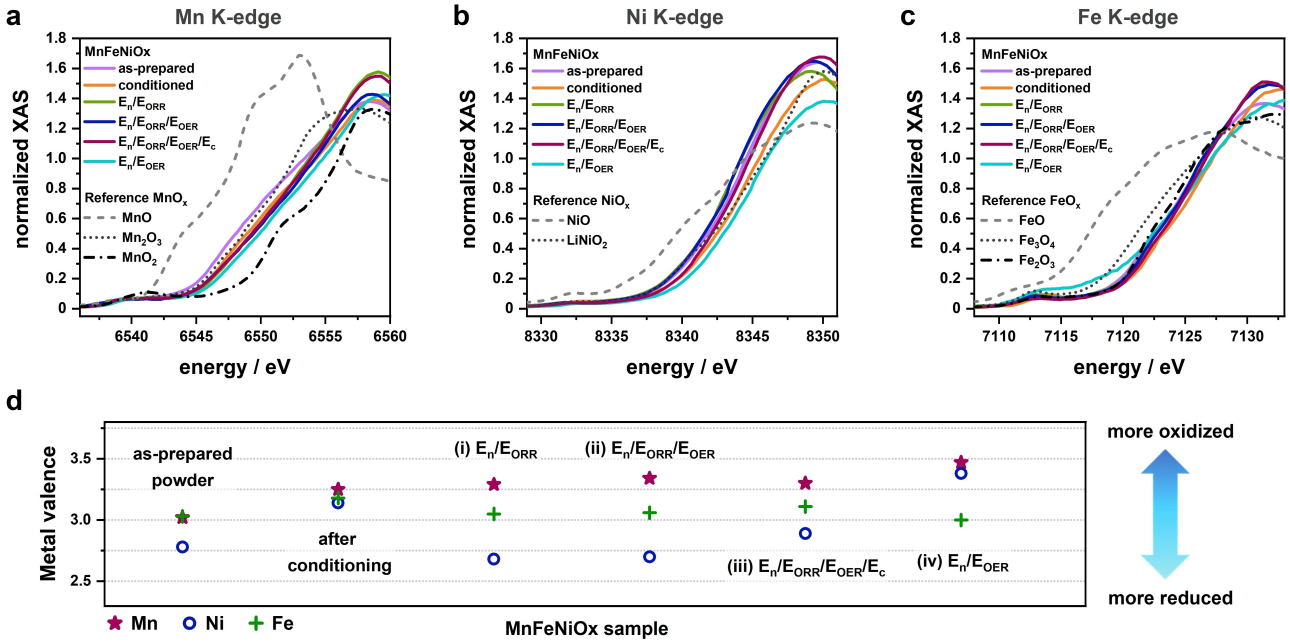

Figure 6. XANES spectra of (a) Mn–K edge, (b) Ni K-edge, and (c) Fe K-edge recorded on MnFeNiOx, as prepared, after conditioning step, and after various chronoamperometric test sequences conducted in air-saturated 0.1 M KOH. XAS spectra were collected in fluorescence mode. Potentials (vs RHE) applied were $E_n = 1.20$ V, $E_{ORR} = 0.83$ V, $E_{OER} = 1.52$ V, and $E_c = -0.53$ V. XANES spectra of various metal oxides (MOx, M = Mn, Ni, Fe) are shown in the figures for reference. Estimated valences of (d) Mn, (e) Ni, and (f) Fe in the different MnFeNiOx samples.

Table 1. Mn, Ni and Fe valences (z_M) in MnFeNiOx samples and their corresponding edge energies (E_{edge}) before and after various electrochemical sequences.

Sample	Mn		Ni		Fe	
	E_{edge}/eV	z_{Mn}	E_{edge}/eV	z_{Ni}	E_{edge}/eV	z_{Fe}
As-prepared powder	6548.9	3.0	8342.0	2.8	7123.1	3.0
After conditioning	6549.7	3.2	8342.8	3.1	7123.9	3.2
(i) E_n/E_{ORR}	6549.9	3.3	8341.8	2.7	7123.2	3.0
(ii) $E_n/E_{ORR}/E_{OER}$	6550.1	3.4	8341.8	2.7	7123.3	3.1
(iii) $E_n/E_{ORR}/E_{OER}/E_c$	6549.9	3.3	8342.2	2.9	7123.5	3.1
(iv) E_n/E_{OER}	6550.6	3.5	8343.3	3.4	7123.0	3.0

estimated Mn, Ni and Fe valences are visualized in Figure 6d and summarized in Table 1 for all samples.

After (i) E_n/E_{ORR}, (ii) $E_n/E_{ORR}/E_{OER}$, and (iii) $E_n/E_{ORR}/E_{OER}/E_c$, the three metals clearly displayed changes in their chemical states with respect to the as-prepared MnFeNiOx sample that are different to those observed after conditioning. In the case of Ni and Fe, their highest valence was observed in the samples measured after conditioning, suggesting that these metals are reduced during the chronoamperometric sequences, likely due to the cathodic potential applied during the E_{ORR} step. However, Mn increased slightly its valence from 3.2 after conditioning to 3.3, 3.4 and 3.3 after the sequences (i) E_n/E_{ORR}, (ii) $E_n/E_{ORR}/E_{OER}$, and (iii) $E_n/E_{ORR}/E_{OER}/E_c$, respectively. While this difference can be considered within the method's error (Table S4), it is also plausible that Mn is oxidized during the E_n steps (1.20 V vs RHE) as suggested by the redox features shown in Figure S4, and undergoes further oxidation during the E_{OER} step. Interestingly, no substantial difference was observed between Ni valences after (i) E_n/E_{ORR} and after (ii) $E_n/E_{ORR}/E_{OER}$, while Mn and Fe displayed slightly more oxidized states, which, however, are difficult to distinguish from method's error. This observation correlates with those made in relation to the ORR selectivity of MnFeNiOx (Figure 3d), namely, there was also no substantial difference in the yield of peroxide species after either of the two sequences. Compared to (ii) $E_n/E_{ORR}/E_{OER}$, subjecting MnFeNiOx to the (iii) $E_n/E_{ORR}/E_{OER}/E_c$ sequence leads to a slightly lower Mn valence, the same Fe valence, and an insignificantly higher Ni valence. These results support that, rather than restoring the chemical state of the three metals to match those observed in (i) E_n/E_{ORR} (which was our initial hypothesis), E_c induced a transformation that brought Ni to a higher chemical state, which can be correlated with the increase in the rate of oxygen generation[46] as observed during the (iii) $E_n/E_{ORR}/E_{OER}/E_c$ sequence (Figure 5). Moreover, considering the observed increase in peroxide yield (Figure 3d) after (iii) $E_n/E_{ORR}/E_{OER}/E_c$, it is suggested that not only Mn[30] but also Ni has a strong influence in the selectivity of MnFeNiOx during the ORR, which is in agreement with other works reporting relatively high peroxide yields with Ni-containing ORR catalysts.[47]

To differentiate oxidation due to the conditioning step from oxidation that may take place during the E_{OER} step, in addition to the chronopotentiometric sequences shown in Scheme 1, the catalyst was subjected to a fourth sequence, (iv) E_n/E_{OER}, as illustrated in Scheme S1. As shown in Figure 6d, this sample displayed the most oxidized states for Mn and Ni out of all the investigated MnFeNiOx samples, indicating that oxidation during the conditioning step was milder than during the E_{OER} step for these two metals. Meanwhile, the average valence of Fe after (iv) E_n/E_{OER} was 3.0. In fact, the differences observed in the Fe valences of the various MnFeNiOx samples (all being in the range between 3.0 and 3.2) are difficult to distinguish from the method's error, and were substantially smaller than those observed for Mn (between 3.0 and 3.5) and Ni (between 2.7 and 3.4). These results indicate a high stability (or reversibility) of the Fe species under a wide range of potentials, which renders this metal a particularly interesting component for applications that require dynamic variation of operating conditions. The results obtained by XAS confront our initial hypothesis that the oxidative damage of ORR-active species during the OER is the main cause of activity loss of MnFeNiOx, and that it can be reversed by applying the highly cathodic E_c pulse. In the case of MnFeNiOx, either such damage takes place (likely on the very surface and thus was not possible to observe it clearly with XAS) and it is irreversible, or the cause of the activity loss is of a different nature (for example, corrosion, agglomeration, or detachment of the nanoparticles), or both. We propose that the observed changes in catalyst performance are mainly related to the stability of Mn, since it has been shown in diverse reports that there is a strong correlation between Mn valence and ORR activity.[30, 48] As a case study, the results shown in this work show the complexity of changes that a catalyst may undergo upon exposure to dynamically changing potentials and emphasizes that understanding these changes could further enable the use of dynamic electrochemical treatments for the deliberate recovery and/or enhancement of the catalytic capabilities of functional materials.

Conclusions

We investigated an electrochemical method to restore, *in situ*, the ORR activity of a bifunctional ORR/OER catalyst, MnFeNiOx, which undergoes ORR activation under alternating ORR/OER operating conditions.[10] For this purpose, MnFeNiOx was subjected to different chronoamperometric sequences using a rotating disk electrode (RDE) setup. In these sequences, the

applied potentials were dynamically changed between 2 or more of the following potential steps: E_n (1.2 V vs RHE, a potential where neither the ORR nor the OER take place), E_{ORR} (0.83 V vs RHE, corresponding to a current density of $-1\ mA\,cm^{-2}$), E_{OER} (1.52 V vs RHE, corresponding to a current density of $+1\ mA\,cm^{-2}$), and E_c (cathodic potential pulses in the range between −0.83 and 0.37 V vs RHE). Firstly, the optimal E_c value for MnFeNiOx was estimated via a fast E_c-screening method in which the sequence (iii) $E_n/E_{ORR}/E_{OER}/E_c$ was applied varying the E_c values between 0.37 and −0.53 V vs RHE. Each E_c step was applied for a total of 5 cycles before increasing to the next (more cathodic) value in 100 mV steps. The screening method allowed identifying the potential range in which E_c led to a partial recovery of the ORR current of MnFeNiOx after its exposure to the E_{OER} potentials. We propose that this method can be easily applied to observe, in a single experiment, the effect that a wide range of E_c values have on other bifunctional ORR/OER materials.

Upon optimization of E_c, it was observed that applying the sequence $E_n/E_{ORR}/E_{OER}/E_c$ led to a partial recovery of the currents measured during the E_{ORR} steps. Rotating ring disk electrode (RRDE) voltammetry revealed that applying E_c leads to an increase in the yield of peroxide species formed during the E_{ORR} step. Yet, this sequence ($E_n/E_{ORR}/E_{OER}/E_c$) also led to an enhancement of the OER activity, which was confirmed by an increased amount of oxygen detected during the E_{OER} step. These observations were further correlated to changes in Mn, Ni and Fe valences determined by X-ray absorption spectroscopy, suggesting on the one hand, that both Mn and Ni have a strong impact on the ORR selectivity, and on the other hand, that the decrease in ORR activity at alternating ORR/OER conditions may be related to causes different or additional to oxidative damage of the ORR-active species.

As a case study, this work highlights the importance of (1) conducting electrochemical experiments coupled with the detection of their products to differentiate catalytic currents from other processes, (2) the careful selection of electrode preparation sequences and their impact on the properties of the material under investigation, (3) monitoring catalysts under dynamically changing conditions, which is particularly important for the design of BOEs and other materials whose applications require high reversibility, and (4) understanding the various changes that a catalyst undergoes when exposed to different electrochemical conditions, which can potentially enable routes to *in situ* restore and/or enhance their catalytic properties.

Experimental Section

Synthesis and characterization of MnFeNiOx

Synthesis of MnFeNiOx was conducted as described in a previous work.[10] Firstly, high-quality multiwalled carbon nanotubes were grown by chemical vapor deposition at 680 °C using ethylene as precursor and a FeCo-based growth catalyst.[49] The nanotubes were treated for 4 h in a boiling acid solution (HCl, 15 vol%) under stirring to remove catalysts residues, and subsequently washed with distilled water until pH 7. Catalyst residues were below 0.1 wt % according to previous analyses.[50] Subsequently, the grown carbon nanotubes were treated in concentrated HNO_3 solution for 2 h to obtain oxygen-functionalized carbon nanotubes. After washing with distilled water until pH 7 and drying, the obtained powder was modified with Mn, Fe, and Ni using an aqueous mixture of the corresponding metal nitrates via incipient wetness impregnation, dried at 110 °C for 4 h, and finally annealed at 350 °C for 4 h to form metal oxide nanoparticles with metal composition $Mn_{0.51}Fe_{0.14}Ni_{0.35}$ and a total metal loading of 14.4 wt% according to previous XRF analysis.[10] Structural characterization of the as-prepared MnFeNiOx sample including XRD, high-resolution TEM, XPS, Raman spectroscopy, among others, were reported previously[10] and are summarized in Table S1 (Supporting Information).

Electrochemical measurements

Electrochemical experiments were conducted with an Autolab PGSTAT bipotentiostat/galvanostat (Metrohm) in a three-electrode configuration setup. As working electrode were used either catalyst-modified glassy carbon rotating disk electrodes (RDE) with 0.113 cm^2 geometric area, or rotating ring disk electrodes (RRDE) with a catalyst-modified glassy carbon disk electrode (0.196 cm^2) and a platinum ring electrode (0.153 cm^2). To modify the working electrodes, 5 $mg\,mL^{-1}$ catalyst were dispersed in a mixture of ethanol and water (1:1 volume ratio) containing 2 vol% as-purchased Nafion solution (~5 wt% Nafion in a mixture of alcohols, Sigma-Aldrich) by sonication for 15 min. Subsequently, the volume required to achieve a catalyst loading of 210 $\mu g\,cm^{-2}$ was drop-casted onto the glassy carbon disk electrodes and left to dry at ambient conditions. A platinum mesh was used as the counter electrode, and was kept in a compartment separated by a glass frit during the measurements. A commercial Ag|AgCl|KCl (3 M) double-junction electrode (Metrohm) was used as the reference electrode. All experiments were conducted in 0.1 M KOH aqueous solution saturated either with oxygen or with argon. A stream of the corresponding gas was kept near the surface of the electrolyte during the experiments to maintain gas saturation. Before the measurements, the electrolyte was purified using a Chelex cation-exchange resin (Bio-Rad Laboratories) to remove metal impurities.[51] After setup, as part of the electrode preparation sequence for all measurements, the open circuit potential (OCP) was recorded for 1 min, after which cyclic voltammograms were recorded in the potential range between −0.8 and 0.45 V vs Ag|AgCl|KCl (3 M) at a scan rate of 100 $mV\,s^{-1}$ until unchanging voltammograms were observed. Afterwards, electrochemical impedance spectroscopy (EIS) was conducted in the frequency range from 100 kHz to 1 kHz with an AC amplitude of 10 mV (RMS) at the previously determined OCP value. The uncompensated resistance (R_u) was determined from the resulting Nyquist plots, and it was then used together with the measured current ($i_{measured}$) to correct the measured potentials ($E_{measured}$) according to Equation 1.

$$E_{corrected} = E_{measured} - R_u \cdot i_{measured} \quad (1)$$

Potentials vs Ag|AgCl|KCl (3 M) were converted to the reversible hydrogen electrode (RHE) scale according to Equation 2, using a pH value of 12.9 considering the activity coefficient of the KOH solution.[52]

$$E\ \text{vs RHE} = E\ \text{vs Ag|AgCl|KCl} + 0.207 + 0.059 \cdot \text{pH} \quad (2)$$

The activity of MnFeNiOx towards the hydrogen evolution reaction (HER) was investigated with an RDE setup by recording a linear

sweep voltammogram in the potential range from −0.4 to −1.8 V vs Ag|AgCl|KCl at a scan rate of 5 mV s^{-1} and a rotation rate of 1600 rpm in an Ar-saturated electrolyte.

Four dynamic potential sequences were used according to Scheme 1 and S1, involving the potentials indicated in Table S2. Before each sequence, E_n was held for 150 s. To determine an effective E_c value, the sequence (iii) $E_n/E_{ORR}/E_{OER}/E_c$ was repeatedly conducted using increasingly negative E_c values between −0.6 to −1.5 V vs Ag|AgCl|KCl in 100 mV steps, maintaining each E_c value for 5 cycles. For comparison, (i) E_n/E_{ORR} and (ii) $E_n/E_{ORR}/E_{OER}$ were looped for a total of 100 minutes. After identifying the range of effective E_c potentials, (iii) $E_n/E_{ORR}/E_{OER}/E_c$ was conducted repeatedly at fixed E_c values of −0.9, −1.2, −1.5, and −1.8 V vs Ag|AgCl|KCl for a total of 100 min. These measurements were performed under 1600 rpm electrode rotation in O_2-saturated 0.1 M KOH solution.

The oxygen reduction activity and selectivity were investigated by means of RRDE voltammetry by recording a linear sweep voltammogram in the potential region from 0.23 to −0.9 V vs Ag|AgCl|KCl at a scan rate of 5 mV s^{-1} and rotation rate of 1600 rpm in O_2-saturated electrolyte, while simultaneously applying a constant potential of 0.4 V vs Ag|AgCl|KCl at the Pt ring electrode to oxidize the peroxide species produced at the disk electrode. The voltammograms were recorded before and after conducting the chronoamperometric sequences for a total of 20 cycles applying an E_c value of −1.5 V vs Ag|AgCl|KCl in the case of (iii) $E_n/E_{ORR}/E_{OER}/E_c$. The yield of peroxide species formed during the ORR (HO_2^-) was determined according to Equation 3 considering the background-corrected currents measured at the disk electrode (i_{disk}) and at the ring electrode (i_{ring}), and the collection efficiency factor (N).

$$HO_2^- = \frac{2\left(\frac{i_{ring}}{N}\right)}{i_{disk} + \left(\frac{i_{ring}}{N}\right)} \cdot 100 \quad (3)$$

N was determined experimentally after the measurements for each electrode film by adding 5 mM potassium hexacyanoferrate to the electrolyte and purging it thoroughly with Ar gas to remove oxygen from the solution. Subsequently, a linear sweep voltammogram was recorded at the catalyst-modified disk electrode in the potential region between 0.5 and −0.26 V vs Ag|AgCl|KCl at 5 mV s^{-1} scan rate and 1600 rpm electrode rotation to reduce Fe(III) to Fe(II). Meanwhile, a potential of 0.4 V vs Ag|AgCl|KCl was held at the Pt ring electrode to oxidize the Fe(II) species formed at the disk electrode back to Fe(III). N was then calculated considering the reduction current measured at the disk (i_{red}) and the oxidation current measured at the ring (i_{ox}) according to Equation 4.

$$N = -\frac{i_{ox}}{i_{red}} \quad (4)$$

Experiments for monitoring oxygen formation during the sequences (ii) $E_n/E_{ORR}/E_{OER}$ and (iii) $E_n/E_{ORR}/E_{OER}/E_c$ were conducted in Ar-saturated 0.1 M KOH solution using an RRDE setup for a total of 20 cycles, preceded and followed by an E_n step with a 150 s duration. During the experiments, a rotation rate of 1600 rpm was maintained and a constant potential of −0.7 V vs Ag|AgCl|KCl was applied at the Pt ring electrode to reduce the oxygen that was formed at the disk electrode during the OER.

X-ray absorption spectroscopy (XAS)

Samples for XAS investigations were prepared by drop-casting 10.5 μL catalyst ink onto 5×10 mm^2 glassy carbon plates (HTW Hochtemperatur-Werkstoffe GmbH) covering only about one half of the electrode area. The catalyst inks had the same composition as described for electrochemical experiments. After drying at room conditions, the catalyst-modified plate was used as a working electrode for its electrochemical treatment in air-saturated 0.1 M KOH electrolyte, assembled together with a graphite rod counter electrode and a Ag|AgCl|NaCl (3 M) reference electrode in a 3-electrode configuration setup. Potentials were controlled using a Reference [600]+ potentiostat (Gamry). Cyclic voltammograms were recorded in the potential range between −0.8 and 0.45 V vs Ag|AgCl|NaCl at 100 mV s^{-1} scan rate until reproducible voltammograms were observed. Subsequently, the electrodes were subjected to one of the chronoamperometric sequences shown in Scheme 1 and S1 for a total of 20 cycles. After this, the electrodes were rinsed with water, dried at room conditions, and used for XAS measurements. Reference metal oxide samples were used without further purification, and included MnO, Mn_2O_3, MnO_2, FeO, Fe_3O_4, $LiNiO_2$ from Sigma-Aldrich; NiO from Carl Roth; Fe_2O_3 from Alfa Aesar. As-prepared MnFeNiOx and reference metal oxide samples were prepared for XAS analysis by homogeneously spreading a thin layer of the corresponding powder onto Kapton tape.

XAS spectra were collected at the KMC-3 beamline at the BESSY II synchrotron (Helmholtz-Zentrum Berlin für Materialien und Energie) at room temperature.[53] The beamline is equipped with a double-crystal Si (111) monochromator. Spectra were recorded in fluorescence mode in the Mn–K, Ni–K and Fe–K edges using a 13-element silicon drift detector (RaySpec). The energy was calibrated by positioning the first peak of the first derivative of Co reference foil spectra to the reported energies of 7709 eV,[54] with an accuracy ±0.1 eV. XAS spectra were recorded at least in triplicate for each of the samples to a k-space of 12 Å^{-1}. Data analysis was done as described step-by-step in the supporting information of a previous report.[24] In short, normalization of the recorded spectra was done by subtracting a straight line obtained by the linear fit of the measured data before the corresponding K edge. Subsequently, the resulting spectra was divided by the polynomial function (order 2) obtained by fitting the data after the K edge. The edge energy (E_{edge}) of reference samples was determined by the step integral method proposed by Dau *et al.*[45] according to Equation 5, using $\mu_1 = 0.15$ and $\mu_2 = 1$.

$$E_{edge} = E_1 + \frac{1}{\mu_2 - \mu_1}\int_{E_1}^{E_2} \mu_2 - \tilde{\mu}(E)dE \quad (5)$$

The E_{edge} values obtained for reference metal oxide samples were used to build metal valence vs edge energy plots (Figure S5), which were later fitted to a straight line to obtain Equations 6, 7 and 8. These curves were later used to estimate the valence (z_M) of M = Mn, Fe and Ni in the different MnFeNiOx samples with their corresponding E_{edge} values. All values are summarized in Table S4.

$$z_{Mn} = 0.2682 \cdot E_{edge} - 1753.39105 \quad (6)$$

$$z_{Fe} = 0.1952 \cdot E_{edge} - 1387.40064 \quad (7)$$

$$z_{Ni} = 0.46813 \cdot E_{edge} - 3902.35909 \quad (8)$$

The coefficients of determination R^2 corresponding to the linear fits were 0.99143, 0.99209 and 1, respectively. Note that the equations were obtained with 3, 3 and 2 points, respectively.

Acknowledgements

The authors are grateful to Denis Antipin, Joaquín Morales-Santelices, Dr. Max Baumung (Nachwuchsgruppe Gestaltung des Sauerstoffentwicklungsmechanismus, Helmholtz-Zentrum Berlin), and to beamline scientists Dr. Paul Beyer (Department of Physics, Freie Universität Berlin), Dr. Michael Haumann (Department of Physics, Freie Universität Berlin) and Dr. Ivo Zizak (Abteilung Struktur und Dynamik von Energiematerialien, Helmholtz-Zentrum Berlin für Materialien und Energie) for their support during the collection of XAS data, as well as to Dr. Patrick Wilde (Analytical Chemistry, Ruhr University Bochum) for preliminary TEM measurements. We thank HZB for the allocation of synchrotron radiation beamtime at BESSY II. D.M.M. is grateful for the financial support of DFG in the framework of SPP 2080 "DynaKat" Early Career Research Scholarships for Female Scientists. This project has received funding from the European Research Council (ERC) under the European Union's Horizon 2020 research and innovation programme under grant agreement No 804092.

Conflict of Interests

The authors declare no conflict of interest.

Data Availability Statement

The data that support the findings of this study are available from the corresponding author upon reasonable request.

Keywords: bifunctional oxygen electrodes · dynamic operating conditions · rotating ring disk electrode · transition metals · X-ray absorption spectroscopy

[1] X. Wu, C. Tang, Y. Cheng, X. Min, S. P. Jiang, S. Wang, *Chem. Eur. J.* **2020**, *26*, 3906–3929.
[2] a) R. A. Rincon, J. Masa, S. Mehrpour, F. Tietz, W. Schuhmann, *Chem. Commun.* **2014**, *50*, 14760–14762; b) H. Zhong, R. Tian, X. Gong, D. Li, P. Tang, N. Alonso-Vante, Y. Feng, *J. Power Sources* **2017**, *361*, 21–30; c) J. Masa, W. Xia, I. Sinev, A. Zhao, Z. Sun, S. Grützke, P. Weide, M. Muhler, W. Schuhmann, *Angew. Chem. Int. Ed.* **2014**, *53*, 8508–8512.
[3] S. Zhao, L. Yan, H. Luo, W. Mustain, H. Xu, *Nano Energy* **2018**, *47*, 172–198.
[4] a) Y. Zhu, C. Su, X. Xu, W. Zhou, R. Ran, Z. Shao, *Chem. Eur. J.* **2014**, *20*, 15533–15542; b) F. D. Kong, S. Zhang, G. P. Yin, N. Zhang, Z. B. Wang, C. Y. Du, *J. Power Sources* **2012**, *210*, 321–326; c) G. Zhang, Z.-G. Shao, W. Lu, G. Li, F. Liu, B. Yi, *Electrochem. Commun.* **2012**, *22*, 145–148; d) F. D. Kong, S. Zhang, G. P. Yin, Z. B. Wang, C. Y. Du, G. Y. Chen, N. Zhang, *Int. J. Hydrogen Energy* **2012**, *37*, 59–67.
[5] a) H. Osgood, S. V. Devaguptapu, H. Xu, J. Cho, G. Wu, *Nano Today* **2016**, *11*, 601–625; b) K. Zeng, X. Zheng, C. Li, J. Yan, J.-H. Tian, C. Jin, P. Strasser, R. Yang, *Adv. Funct. Mater.* **2020**, *30*, 2000503.
[6] a) K. B. Ibrahim, M.-C. Tsai, S. A. Chala, M. K. Berihun, A. W. Kahsay, T. A. Berhe, W.-N. Su, B.-J. Hwang, *J. Chin. Chem. Soc.* **2019**, *66*, 829–865; b) Y.-J. Wang, B. Fang, D. Zhang, A. Li, D. P. Wilkinson, A. Ignaszak, L. Zhang, J. Zhang, *Electrochem. Energy Rev.* **2018**, *1*, 1–34; c) G. Fu, Y. Tang, J.-M. Lee, *ChemElectroChem* **2018**, *5*, 1424–1434.
[7] W. Zhu, R. Zhang, F. Qu, A. M. Asiri, X. Sun, *ChemCatChem* **2017**, *9*, 1721–1743.
[8] a) G. Fu, X. Jiang, Y. Chen, L. Xu, D. Sun, J.-M. Lee, Y. Tang, *NPG Asia Mater.* **2018**, *10*, 618–629; b) W. Zhao, F. Wu, H. Wu, G. Chen, *J. Nanomater.* **2010**, *2010*, 1–5.
[9] a) S. Liu, M. Liu, X. Li, S. Yang, Q. Miao, Q. Xu, G. Zeng, *Carbon Energy* **2023**, *5*; b) Y. Li, M. Cui, Z. Yin, S. Chen, T. Ma, *Chem. Sci.* **2020**, *11*, 11646–11671.
[10] D. M. Morales, M. A. Kazakova, S. Dieckhöfer, A. G. Selyutin, G. V. Golubtsov, W. Schuhmann, J. Masa, *Adv. Funct. Mater.* **2020**, *30*, 1905992.
[11] M. A. Kazakova, D. M. Morales, C. Andronescu, K. Elumeeva, A. G. Selyutin, A. V. Ishchenko, G. V. Golubtsov, S. Dieckhöfer, W. Schuhmann, J. Masa, *Catal. Today* **2020**, *357*, 259–268.
[12] M. Wu, G. Zhang, Y. Hu, J. Wang, T. Sun, T. Regier, J. Qiao, S. Sun, *Carbon Energy* **2021**, *3*, 176–187.
[13] a) G. Fu, X. Yan, Y. Chen, L. Xu, D. Sun, J.-M. Lee, Y. Tang, *Adv. Mater.* **2018**, *30*; b) G. Fu, Y. Liu, Y. Chen, Y. Tang, J. B. Goodenough, J.-M. Lee, *Nanoscale* **2018**, *10*, 19937–19944; c) X. Hu, Y. Chen, M. Zhang, G. Fu, D. Sun, J.-M. Lee, Y. Tang, *Carbon* **2019**, *144*, 557–566.
[14] D. M. Morales, M. A. Kazakova, M. Purcel, J. Masa, W. Schuhmann, *J. Solid State Electrochem.* **2020**, *50*, 14760.
[15] a) R. D. McKerracher, H. A. Figueredo-Rodríguez, C. Ponce de León, C. Alegre, V. Baglio, A. S. Aricó, F. C. Walsh, *Electrochim. Acta* **2016**, *206*, 127–133; b) S. Dresp, F. Luo, R. Schmack, S. Kühl, M. Gliech, P. Strasser, *Energy Environ. Sci.* **2016**, *9*, 2020–2024.
[16] K. F. Kalz, R. Kraehnert, M. Dvoyashkin, R. Dittmeyer, R. Gläser, U. Krewer, K. Reuter, J.-D. Grunwaldt, *ChemCatChem* **2017**, *9*, 17–29.
[17] a) L. Li, A. Manthiram, *Nano Energy* **2014**, *9*, 94–100; b) M. Xiong, M. P. Clark, M. Labbe, D. G. Ivey, *J. Power Sources* **2018**, *393*, 108–118.
[18] C. Alegre, C. Busacca, A. Di Blasi, O. Di Blasi, A. S. Aricò, V. Antonucci, V. Baglio, *Mater. Today Energy* **2020**, *18*, 100508.
[19] a) N. Sikdar, P. Schwiderowski, D. Medina, S. Dieckhöfer, T. Quast, A. C. Brix, S. Cychy, M. Muhler, J. Masa, W. Schuhmann, *ChemElectroChem* **2021**, *8*, 1685–1693; b) M. S. Ahmed, B. Choi, Y.-B. Kim, *Sci. Rep.* **2018**, *8*, 2543.
[20] M. A. Kazakova, A. Koul, G. V. Golubtsov, A. G. Selyutin, A. V. Ishchenko, R. I. Kvon, B. A. Kolesov, W. Schuhmann, D. M. Morales, *ChemElectroChem* **2021**, *8*, 2803–2816.
[21] a) S. Gupta, S. Zhao, X. X. Wang, S. Hwang, S. Karakalos, S. V. Devaguptapu, S. Mukherjee, D. Su, H. Xu, G. Wu, *ACS Catal.* **2017**, *7*, 8386–8393; b) K. Li, M. Yin, Z. Wang, X. Chen, T. Zhu, J. Wang, N. Dewangan, Y. Yu, Q. Zhong, S. Kawi, *ChemistrySelect* **2018**, *3*, 12424–12429.
[22] a) S. Barwe, J. Masa, C. Andronescu, B. Mei, W. Schuhmann, E. Ventosa, *Angew. Chem. Int. Ed.* **2017**, *56*, 8573–8577; b) M. R. Mohammadi, S. Loos, P. Chernev, C. Pasquini, I. Zaharieva, D. González-Flores, P. Kubella, K. Klingan, R. D. L. Smith, H. Dau, *ACS Catal.* **2020**, *10*, 7990–7999; c) D. A. Lutterman, Y. Surendranath, D. G. Nocera, *J. Am. Chem. Soc.* **2009**, *131*, 3838–3839; d) A. E. Thorarinsdottir, S. S. Veroneau, D. G. Nocera, *Nat. Commun.* **2022**, *13*, 1243.
[23] H. A. El-Sayed, A. Weiß, L. F. Olbrich, G. P. Putro, H. A. Gasteiger, *J. Electrochem. Soc.* **2019**, *166*, F458–F464.
[24] J. Villalobos, R. Golnak, L. Xi, G. Schuck, M. Risch, *J. Phys. Energy* **2020**, *2*, 34009.
[25] R. Tang-Kong, C. E. D. Chidsey, P. C. McIntyre, *J. Electrochem. Soc.* **2019**, *166*, H712–H717.
[26] D. Medina, T. Löffler, D. M. Morales, J. Masa, T. Bobrowski, S. Barwe, C. Andronescu, W. Schuhmann, *Electrochem. Commun.* **2021**, *124*, 106960.
[27] J. Hao, W. Luo, S. Wang, K. Zhao, J. Hou, L. Li, B. Ge, W. Yang, W. Shi, *Angew. Chem. Int. Ed.* **2021**, *60*, 20042–20048.
[28] N. Yamada, S. Kitano, Y. Yato, D. Kowalski, Y. Aoki, H. Habazaki, *ACS Appl. Energ. Mater.* **2020**, *3*, 12316–12326.
[29] W. Cheng, S. Xi, Z.-P. Wu, D. Luan, X. W. D. Lou, *Sci. Adv.* **2021**, *7*, eabk0919.
[30] D. M. Morales, J. Villalobos, M. A. Kazakova, J. Xiao, M. Risch, *ChemElectroChem* **2021**, *8*, 2979–2983.
[31] a) W. Chen, Q. Xiang, T. Peng, C. Song, W. Shang, T. Deng, J. Wu, *iScience* **2020**, *23*, 101532; b) K. J. J. Mayrhofer, D. Strmcnik, B. B. Blizanac, V. R. Stamenkovic, M. Arenz, N. M. Markovic, *Electrochim. Acta* **2008**, *53*, 3181–3188.
[32] M. Risch, *Curr. Opin. Electrochem.* **2023**, *38*, 101247.
[33] D. Medina, PhD thesis, Ruhr-Universität Bochum (Germany), **2020**.
[34] T. Löffler, A. Ludwig, J. Rossmeisl, W. Schuhmann, *Angew. Chem. Int. Ed.* **2021**.
[35] A. R. Zeradjanin, *ChemSusChem* **2018**, *11*, 1278–1284.

[36] Z. Wang, X. Guo, J. Montoya, J. K. Nørskov, *NPJ Comput. Mater.* **2020**, *6*, 160.
[37] R. Gao, M. Deng, Q. Yan, Z. Fang, L. Li, H. Shen, Z. Chen, *Small Methods* **2021**, *5*, e2100834.
[38] M. E. G. Lyons, L. Russell, M. O'Brien, R. L. Doyle, I. Godwin, M. P. Brandon, *Int. J. Electrochem. Sci.* **2012**, *7*, 2710–2763.
[39] M. E. G. Lyons, R. L. Doyle, M. P. Brandon, *Phys. Chem. Chem. Phys.* **2011**, *13*, 21530–21551.
[40] H. Radinger, P. Connor, R. Stark, W. Jaegermann, B. Kaiser, *ChemCatChem* **2021**, *13*, 1175–1185.
[41] K. Zhu, F. Shi, X. Zhu, W. Yang, *Nano Energy* **2020**, *73*, 104761.
[42] a) Z. Zheng, D. Wu, G. Chen, N. Zhang, H. Wan, X. Liu, R. Ma, *Carbon Energy* **2022**, *4*, 901–913; b) S. Hirai et al., *J. Mater. Chem. A* **2018**, *6*, 15102–15109.
[43] a) L. Köhler, L. Szabadics, C. Jooss, M. Risch, *Batteries & Supercaps* **2019**, *2*, 364–372; b) W. Chen, H. Wang, Y. Li, Y. Liu, J. Sun, S. Lee, J.-S. Lee, Y. Cui, *ACS Cent. Sci.* **2015**, *1*, 244–251.
[44] M. Risch, D. M. Morales, J. Villalobos, D. Antipin, *Angew. Chem. Int. Ed.* **2022**, *61*, e202211949.
[45] H. Dau, P. Liebisch, M. Haumann, *Anal. Bioanal. Chem.* **2003**, *376*, 562–583.
[46] Y. Bai et al., *Nat. Commun.* **2022**, *13*, 6094.
[47] a) R. Li et al., *Cell Rep. Phys. Sci.* **2022**, *3*, 100788; b) D. M. Morales, S. Barwe, E. Vasile, C. Andronescu, W. Schuhmann, *ChemPhysChem* **2019**, *20*, 3030–3036; c) P. Liu, J. Ran, B. Xia, S. Xi, D. Gao, J. Wang, *Nano-Micro Lett.* **2020**, *12*, 68.
[48] a) V. Celorrio, A. S. Leach, H. Huang, S. Hayama, A. Freeman, D. W. Inwood, D. J. Fermin, A. E. Russell, *ACS Catal.* **2021**, 6431–6439; b) V. Celorrio, L. Calvillo, G. Granozzi, A. E. Russell, D. J. Fermin, *Top. Catal.* **2018**, *61*, 154–161; c) J. Heese-Gärtlein, D. M. Morales, A. Rabe, T. Bredow, W. Schuhmann, M. Behrens, *Chem. Eur. J.* **2020**; d) Y. Gorlin, B. Lassalle-Kaiser, J. D. Benck, S. Gul, S. M. Webb, V. K. Yachandra, J. Yano, T. F. Jaramillo, *J. Am. Chem. Soc.* **2013**, *135*, 8525–8534.
[49] a) S. N. Bokova-Sirosh, V. L. Kuznetsov, A. I. Romanenko, M. A. Kazakova, D. V. Krasnikov, E. N. Tkachev, Y. I. Yuzyuk, E. D. Obraztsova, *J. Nanophotonics* **2016**, *10*, 12526; b) A. S. Andreev, D. V. Krasnikov, V. I. Zaikovskii, S. V. Cherepanova, M. A. Kazakova, O. B. Lapina, V. L. Kuznetsov, J.-B. d'Espinose de Lacaillerie, *J. Catal.* **2018**, *358*, 62–70.
[50] V. L. Kuznetsov et al., *Phys. Status Solidi B* **2010**, *247*, 2695–2699.
[51] A. Wuttig, Y. Surendranath, *ACS Catal.* **2015**, *5*, 4479–4484.
[52] J. N. Hausmann, B. Traynor, R. J. Myers, M. Driess, P. W. Menezes, *ACS Energy Lett.* **2021**, *6*, 3567–3571.
[53] G. Schuck, I. Zisak, *JLSRF* **2020**, *6*, A139.
[54] J. A. Bearden, A. F. Burr, *Rev. Mod. Phys.* **1967**, *39*, 125–142.

Manuscript received: September 20, 2023
Revised manuscript received: January 28, 2024
Accepted manuscript online: February 1, 2024
Version of record online: February 21, 2024